AIAA JOURNAL
Vol. 47, No. 7, July 2009

Optimal Morphing-Wing Design Using Parallel Nondominated Sorting Genetic Algorithm II

Smita Bharti*
Bucknell University, Lewisburg, Pennsylvania 17837
and
Mary Frecker† and George Lesieutre‡
Pennsylvania State University, University Park, Pennsylvania 16802

DOI: 10.2514/1.36003

The focus of this paper is an optimal design of morphing aircraft wings employing a wing structure composed of an internal layout of cables and struts. Cables are used to provide actuation and stiffness, and struts provide stiffness without actuation. Topology optimization is used to place cables and struts in a bay or a section of the wing. Nonlinear finite element analysis is used to capture the large deformations of the structure, and the optimization is achieved using the Nondominated Sorting Genetic Algorithm II. The optimization procedure is illustrated using a morphing-wing example. The effect of the upper limit on actuation forces is studied, and solutions are found with good agreement between the desired and obtained deflections under actuation and aerodynamic loads. The implemented parallelized optimization algorithm is successful in solving a computationally intense, multi-objective, multiconstraint problem with a large number of discrete and continuous design variables in a reasonable amount of time.

Nomenclature

A_0	=	cross-sectional area
b_1, b_2, b_3	=	strain displacement relationships
C	=	proportionality constant
dU	=	update in displacement
E	=	Young's modulus
F	=	internal forces
F_{act}	=	actuation forces
f_1	=	least-squares error between deflection under actuation and the desired deflection under actuation and airloads
f_2	=	least-squares error between the deflection under airloads and the original undeformed configuration
g_1, g_2, g_3, g_4, g_5	=	constraint sets 1, 2, 3, 4, and 5
$g_{1\text{allow}}, g_{2\text{allow}}, g_{3\text{allow}}, g_{4\text{allow}}, g_{5\text{allow}}$	=	allowable limit on constraints 1, 2, 3, 4, and 5
i	=	varies from 1 to the number of nodes n
j	=	varies from 1 to the number of elements
K	=	stiffness matrix
K_t	=	tangent stiffness matrix
K_{t1}, K_{t2}, K_{t3}	=	components of the tangent stiffness matrix
$l_{\text{cab}_{\text{final}}}$	=	final cable length
$K_{t\sigma}$	=	stress stiffness matrix
$l_{\text{cab}_{\text{initial}}}$	=	initial cable length
l_n	=	final length
l_0	=	initial length
n	=	number of controlled output points (nodes) along the wing boundary
p	=	vector of nodal displacements $(u_1, v_1, w_1, u_2, v_2, w_2)$
q	=	internal forces
R	=	external forces
U	=	nodal deflections
V	=	applied actuation
V_{active}	=	total volume of active members
V_{passive}	=	total volume of passive elements
V_{total}	=	total volume of all structural members
w	=	weighing factor (ranging between 0 and $\frac{1}{2}$)
x	=	upper limit on the fraction of total volume that may be composed of active material
$x_{\text{def act air}}, y_{\text{def act air}}, z_{\text{def act air}}$	=	coordinates of output points when subjected to cable actuation and airloads
$x_{\text{def air}}, y_{\text{def air}}, z_{\text{def air}}$	=	coordinates of the output points when subjected to only airloads and no actuation
$x_{\text{des}}, y_{\text{des}}, z_{\text{des}}$	=	desired deformed coordinates of the output point
$x_{\text{orig}}, y_{\text{orig}}, z_{\text{orig}}$	=	undeformed coordinates of the output point
x_1	=	vector of nodal coordinates $(x_1, y_1, z_1, x_2, y_2, z_2)$
y	=	lower limit on the fraction of total volume which must be composed of passive material
α_0	=	half of the element length $(l_0/2)$
${}^{i}\Delta q^0$	=	starting point of Δq at iteration i
${}^{i-1}\Delta q$	=	converged value of Δq at $(i-1)$th iteration
${}^{i-2}\Delta q$	=	converged value of Δq at $(i-2)$th iteration
ε_{act}	=	strain due to actuation
ε_G	=	Green's strain
σ	=	stress
σ_{act}	=	stress due to actuation
σ_i	=	stress in element i

Received 3 December 2007; revision received 3 March 2009; accepted for publication 3 March 2009.

*Visiting Assistant Professor, Mechanical Engineering.
†Professor, Department of Mechanical and Nuclear Engineering.
‡Professor and Head, Department of Aerospace Engineering. Fellow AIAA.

$\sigma_{\text{yield},i}$ = yield stress of the ith element (strut or cable material)

I. Introduction

SOME aircraft require high maneuverability to perform their designated missions. An additional important goal in current aircraft research is achieving optimal performance in different flight conditions. Maneuverability typically involves (rapid) changes to the wing cross section, and efficiency over a broad range of flight conditions could also involve (slow) changes to the wing planform. Shape change in conventional aircraft wings is accomplished by using control surfaces connected with hinged and sliding joints for yaw, pitch, and roll control. Geometric discontinuities on the wing surface are generally undesirable, because they can disrupt the airflow, thereby introducing undesired drag. By using a smoothly morphing wing, a higher maximum lift coefficient and somewhat lower drag may be achieved. The effectiveness of such a continuously morphing aircraft wing has been demonstrated by the Smart Wing Program [1,2]. In this project, quantitative data were generated to show that significant performance improvements can be achieved by using hingeless alternatives to control surfaces such as flaps and ailerons. The main goals of the current research are to eliminate the geometric discontinuities and to achieve high maneuverability through continuous morphing of an aircraft wing. Additionally, a smooth planform change is sought to maintain flight efficiency over a range of airspeeds.

The key concept in the current work is to achieve continuous wing morphing by using an optimized internal wing structure of struts and tendons (or cables) [3]. Tendons are reeled in or shortened by actuators, and struts provide rigidity against the aerodynamic loads. Wing morphing is pursued in terms of a prescribed shape change, which is modeled as deflection of points on the wing in specified directions. A primary objective is to design an optimal cable-actuated structure to achieve the desired shape change. This wing shape change may be fairly large, depending on the problem at hand.

To fully realize this concept, a three-step design procedure is required: the first step involves designing an optimal internal structure that provides the desired wing deformation, the second step involves identifying a means of actuation, and the third step involves the development of an adequate skin that can morph with the internal structure as well as withstand the aerodynamic loads. In this paper, the first design step is addressed: that of obtaining an optimal cable and strut layout in the wing.

The hyper-elliptic camber section (HECS) wing is used as a sample problem in this research. The HECS wing is designed to provide an improved lift-to-drag ratio over a wide range of angles of attack compared with the planar elliptical baseline [4].

The tendon-actuated wing structure will be composed of a combination of optimally placed tendons or cables and trusses. Figure 1a shows an example of a discretized HECS wing structure, and Fig. 1b shows a sample optimal topology for one section or bay of the wing. The far left end is constrained from motion, and the desired deflections of the nodes at the right end have been specified. The optimal topology is obtained by carrying out a topology optimization on a ground structure (initial layout) consisting of randomly placed truss, cable, and void elements. Voids indicate the absence of truss or cable members at that particular location. They are used to simplify the topology. The goal of topology optimization is to obtain an optimal layout and number of trusses, cables, and voids in the final topology, such that the desired wing morphing is achieved. The example topology shown in Fig. 1b has five actuating cables (shown in black). All elements are modeled as three-dimensional truss elements. Stiff nondesign elements (shown in light gray in Fig. 1b) are the elements that are not allowed to change during the optimization. These might be used, for example, to model a rib that ensures that the cross-sectional shape of the wing does not change significantly. In this research, each bay or section of the wing is designed separately.

The organization of this paper is as follows. Section II provides the problem formulation. The parallelized optimization algorithm is discussed in Sec. III. Nonlinear finite element analysis (FEA) and the convergence of the Newton–Raphson (N-R) iterations are discussed in Sec. IV. Finally, Sec. V describes the optimization results for the HECS wing.

II. Problem Formulation

The general optimization problem is formulated as shown next:

$$\text{Minimize } f_1, f_2 \tag{1}$$

$$\text{Subject to } g_{1\text{–}5} \leq g_{1\text{–}5\text{allow}} \tag{2}$$

where f_1 and f_2 are objectives, and g_1, g_2, g_3, g_4, and g_5 are constraints.

This problem has multiple conflicting objectives. The morphing wing must be flexible under actuation forces and stiff under aerodynamic loads. Flexibility under actuation is quantitatively expressed as the least-squares error between the deflection of the output nodes under the combined effect of actuation and airloads and the desired deflection [Eq. (3)]. Such a formulation ensures that the wing deforms the required amount under actuation forces. Similarly, stiffness under aerodynamic loads may be achieved by minimizing the least-squares error between the deflection of the wing under airloads and the unmorphed configuration of the wing [Eq. (4)]. This ensures that the wing does not deform excessively under airloads alone. The functions are given in Eqs. (3) and (4). Equation (4) may be taken as a rough indicator of aeroelastic issues, in that a stiffer wing will be less susceptible to divergence and flutter:

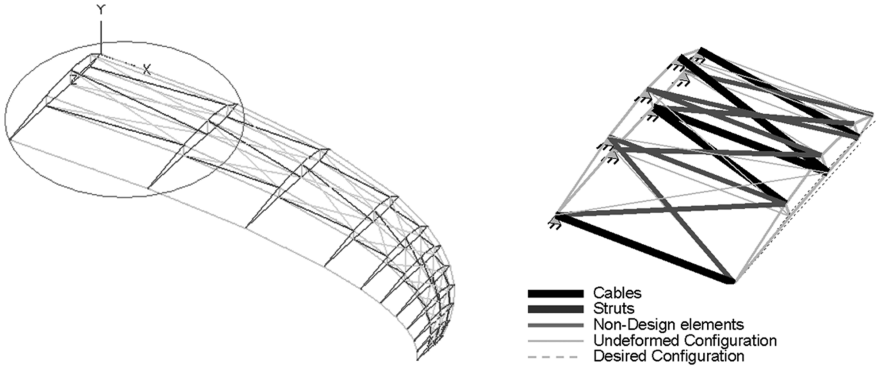

a) Discretized wing structure **b) Sample topology**

Fig. 1 Tendon-actuated wing concept.

$$f_1 = \frac{1}{n}\sum_{i=1}^{n}\sqrt{(x_{\text{def act air},i} - x_{\text{des},i})^2 + (y_{\text{def act air},i} - y_{\text{des},i})^2 + (z_{\text{def act air},i} - z_{\text{des},i})^2} \tag{3}$$

$$f_2 = \frac{1}{n}\sum_{i=1}^{n}\sqrt{(x_{\text{def air},i} - x_{\text{orig},i})^2 + (y_{\text{def air},i} - y_{\text{orig},i})^2 + (z_{\text{def air},i} - z_{\text{orig},i})^2} \tag{4}$$

These equations involve calculations of nodal deflections obtained using nonlinear FEA. Cable actuation forces are modeled in the FEA by shrinking the cable elements. Computational fluid dynamics was used to predict the aerodynamic loads acting on the HECS wing [4].

The stresses in the cables and struts under defined limit-load cases must be less than the yield stress of the material. In the current work, the cables are assumed to be made of stainless steel 304 (yield stress is 517 MPa) and struts of aluminum 7075 T6 (yield stress is 505 MPa). The equation quantitatively expressing the stress limit requirement is given in Eq. (5):

$$\sigma_j \le \sigma_{\text{yield},j} \quad \text{or} \quad g_1 = \frac{\sigma_j}{\sigma_{\text{yield},j}} - 1 \tag{5}$$

In addition to these design requirements, an additional material volume constraint is implemented to prevent the presence of an excessive number of cables and struts in the wing. The volume constraint on cables is used to reduce the number of actuators, and the volume constraint on struts is used to control the weight of the internal wing structure. Hence, Eqs. (6) and (7) must be satisfied:

$$V_{\text{active}} \le \frac{x}{100} V_{\text{total}} \quad \text{or} \quad g_2 = \frac{V_{\text{active}}}{0.01 x V_{\text{total}}} - 1 \tag{6}$$

$$V_{\text{passive}} \le \frac{y}{100} V_{\text{total}} \quad \text{or} \quad g_3 = \frac{V_{\text{passive}}}{0.01 y V_{\text{total}}} - 1 \tag{7}$$

The nonlinear finite element method has been used for solving for the nodal deflections. Section IV discusses the nonlinear FEA in detail. An additional check for stability of the design has been included in the constraints by ensuring the positive definiteness of the stiffness matrix K obtained from the nonlinear FEA. Thus, the following equation must be valid:

$$\text{eigenvalues } (K) \ge 0 \quad \text{or} \quad g_4 = \text{eigenvalues } (K) \tag{8}$$

The last constraint [Eq. (9)] ensures that the cables shorten. Although an elongating cable can provide stiffness to the wing topology, it cannot be used as an actuator. Enforcing the constraint shown in Eq. (9) ensures that only the cables that provide stiffness as well as actuation are present in the topology:

$$l_{\text{cab}_{\text{final}}} - l_{\text{cab}_{\text{initial}}} < 0 \quad \text{or} \quad g_5 = l_{\text{cab}_{\text{initial}}} - l_{\text{cab}_{\text{final}}} \tag{9}$$

The unmorphing, or returning the wing to its original configuration, is an additional important problem that must be addressed. Unmorphing could potentially require additional antagonistic cables or a spring mechanism. However, in this paper, the unmorphing problem is not considered to reduce the number of design variables. A spring mechanism for unmorphing has been implemented in a related work [5].

This is a mixed-variable optimization problem. The discrete variables are the type of each element in the ground structure: cable, strut, or void. By allowing for the possibility of void elements, topology optimization is achieved (i.e., the placements of cables, struts, and voids in the wing body are optimized). Thus, each of the discrete variables can either be 0, 1, or 2, depending on whether it is a void, strut, or cable, respectively. The continuous variables are the amount of actuation forces applied on the cables, resulting in the shortening of cables.

Aerodynamic load data for the HECS wing problem were obtained [4]. Prediction of aerodynamic loads associated with changes in the morphing-wing configuration has been considered for the HECS wing before [6]. In their work, Wiggins et al. [6] applied linear aerodynamic theory to the HECS wing configuration at certain morphed positions to predict aerodynamic loads. However, in the current analysis, the aerodynamic loads are assumed to be constant as the wing morphs. This is done mainly to simplify the analysis during optimization. In future work, a subroutine could be developed to recalculate the aerodynamic loads for the next genetic algorithm (GA) generation by using Schrenk's approximation [7] (to obtain the new spanwise load distribution) and a curve fit of two quadratics (to obtain the new chordwise load distribution).

III. Solution: Topology Optimization Using Parallelized GA (NSGA II)

The optimization solution method is the Nondominated Sorting Genetic Algorithm (NSGA II) [8,9]. NSGA II is a genetic algorithm that can be used to solve a multi-objective, multiconstraint, mixed-variable problem. The flow diagram is given in Fig. 2. NSGA II is an elitist strategy, and hence in every generation it sorts the set of solutions according to their fitness (or objective values) and then

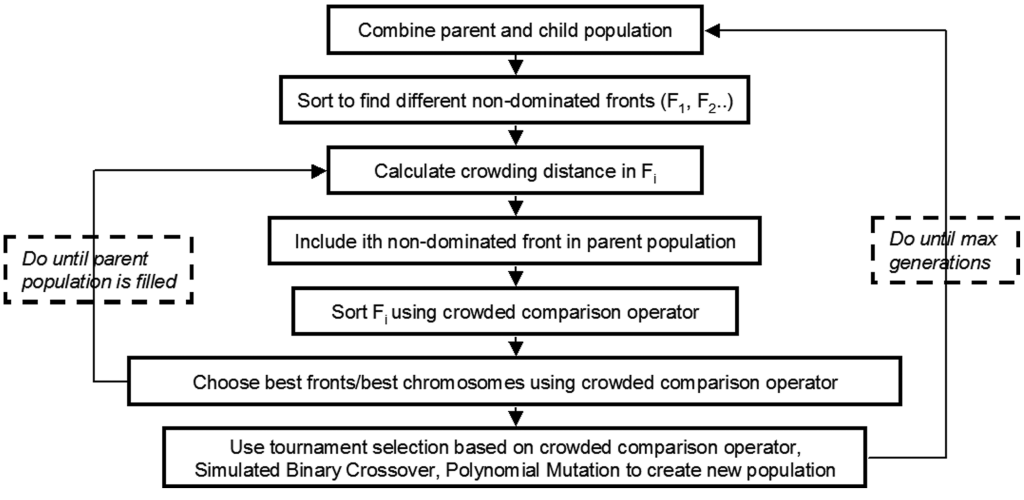

Fig. 2 NSGA II flow diagram.

Table 1 NSGA II parameters

Parameter	Value
Crossover probability	0.7
Probability of real mutation	0.1
Probability of binary mutation	0.01
Crossover type	Single point
Distribution index for crossover	100
Distribution index for mutation	400

selects the best solutions as parents for the next generation. Nondominated Pareto fronts at each generation are found using constraint domination conditions. The parameter values for NSGA II used in the current work are given in Table 1.

In the current algorithm, the fitness function evaluation using nonlinear FEA is very time-consuming, because it involves an iterative FEA procedure inside the GA design iterations. To reduce computation time, a parallel version of NSGA II using a message-passing interface (MPI) [10] has been developed to use multiple nodes to carry out the function evaluations. A master–slave algorithm developed previously [4] is employed in this work. The master processor (Fig. 3) does all the GA operations. The fitness and constraint calculations are performed by the slaves. An asynchronous nonblocking communication using MPI_Irecv and MPI_Waitany is employed to minimize idle time of the nodes. The use of nonblocking communication provides dramatic improvements in the performance of a message-passing algorithm by reducing communication overhead. Once all the function evaluations have been completed by the slaves, the NSGA II proceeds as shown in Fig. 2. The slaves pass on the calculated function values to the master, which then performs all the subsequent GA operations such as selection, crossover, and mutation.

IV. Nonlinear FEA

Nonlinear finite element analysis has been used in the current work to address the large deformation requirements of the problem. Only geometric nonlinearity is considered; the material is assumed to be linear. The total Lagrangian approach is used to solve this problem [11,12].

The basic problem in nonlinear FEA is to find equilibrium deflections and stresses of a body corresponding to the applied loads. The loads acting in the present case are 1) aerodynamic loads, 2) forces due to actuation, and 3) nodal forces corresponding to internal element stresses.

If R is the sum of the aerodynamic loads and forces due to actuation and F is the vector of nodal point forces corresponding to the internal element stresses in a particular wing configuration, nonlinear FEA involves finding values of nodal deflections such that Eq. (10) is satisfied:

$$F - R = 0 \tag{10}$$

Note that the simulation is performed for a particular case of wing morphing under constant-aerodynamic-load conditions. During the genetic algorithm, the actuation forces and nodal point forces corresponding to internal element stresses change. An iterative full Newton–Raphson procedure is used for finding a state of force equilibrium. As a starting point for the nonlinear FEA, an initial guess for nodal displacements U is made. This value is updated until Eq. (10) is satisfied. The flow diagram and the equations used for the nonlinear FEA are given in Appendix A.

Although the Newton–Raphson method is a powerful tool for root finding, due to its quadratic convergence, its success is dependent on finding a good initial guess that is sufficiently close to the final solution. An initial guess that is not close to the final solution can prevent the nonlinear FEA from converging. With the presence of a large number of nodal coordinates, as is the case in the current work, this problem becomes more pronounced.

Various researchers [13–15] have discussed methods to improve the convergence of nonlinear FEA. One scheme involves using the deflection solution from the previous topology iteration as an initial guess for the current nonlinear FEA [14]. A second scheme uses Eq. (11) for obtaining a good starting point for the nodal deflections U at the beginning of the N-R iterations. This equation uses deflection values from previous two generations to obtain a starting U value for the N-R iterations:

$$^{i}\Delta q^{0} = {}^{i-1}\Delta q + w({}^{i-1}\Delta q - {}^{i-2}\Delta q) \tag{11}$$

In the present case, the use of Eq. (11) considerably improved the convergence of the nonlinear FEA. The nonlinear FEA iterations showed a 99.73% convergence with the scheme and a 78% convergence without the scheme. Hence, Eq. (11) was used in the current work to find the initial guess for the nonlinear FEA.

V. HECS Wing Results

As mentioned previously, the HECS wing has been used as an example problem for this work. This wing in its morphed configuration is shown in Fig. 4.

The initial ground structure of the HECS wing consists of 46 elements. Thus, the problem has 50 constraints: 46 uniaxial stress constraints on the elements that ensure that the stresses in all the

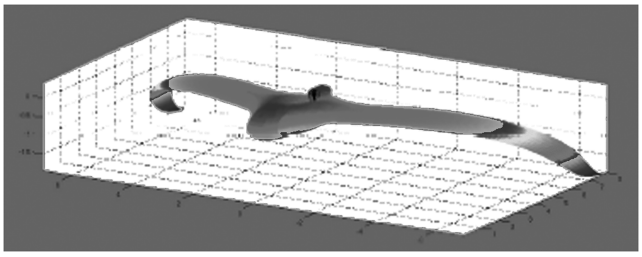

Fig. 4 HECS wing (figure courtesy of NASA Langley Research Center).

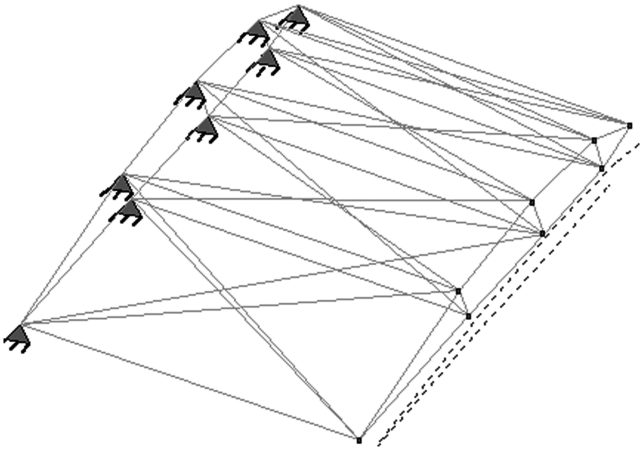

Fig. 5 HECS wing initial ground structure.

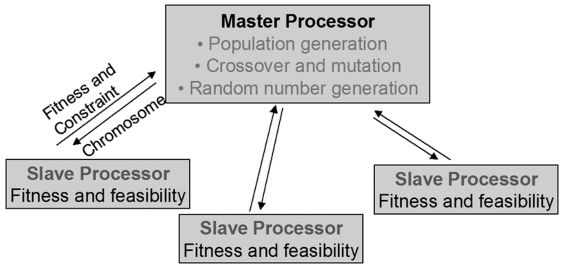

Fig. 3 Master–slave implementation of NSGA II [3].

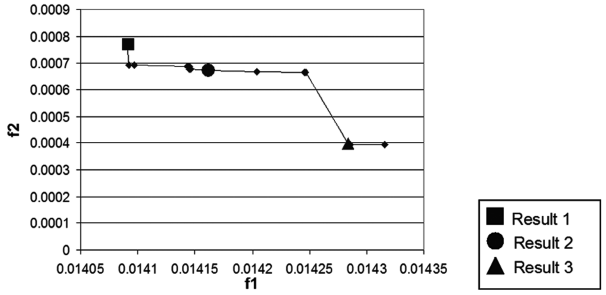

a) Pareto front

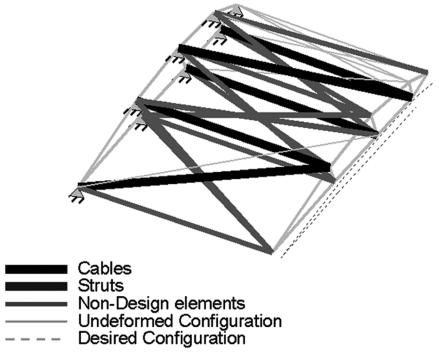

b) Result 1

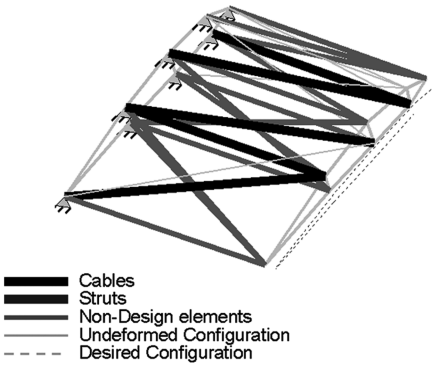

c) Result 2

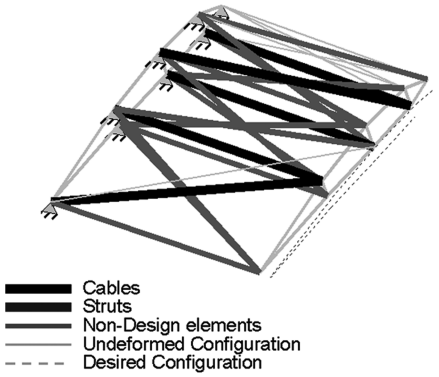

d) Result 3

Fig. 6 Results from case I.

nonvoid elements lie below their yield stresses, 2 volume constraints, 1 constraint that the stiffness matrix is positive definite, and 1 cable-shortening constraint (the shortening of all the cables is considered in a single constraint). The cable volume is constrained to lie below 20% of the total possible volume, and the strut volume is constrained to lie below 50% of the total possible volume. Note that the element cross-sectional areas are not allowed to vary in the optimization algorithm. Hence, the volume constraints limit the number of struts and cables in the optimal topology.

To achieve the desired deflection, a high upper limit on the allowable actuation force must be used. However, using a high upper limit on the allowable actuation force can result in numerical convergence issues. The use of a high actuation-force limit permits cable actuation forces to be an order of magnitude higher than the nodal aerodynamic loads, thereby making the convergence of the nonlinear FEA difficult. This is because Eq. (10) must be satisfied for the iterative nonlinear FEA to converge to a solution. As mentioned in the nonlinear FEA section, using an initial guess for nodal deflections in the Newton–Raphson method that is far from the solution can prevent the convergence of nonlinear FEA. Although the scheme suggested in Eq. (11) helps in the convergence of the nonlinear FEA, an initial guess for the first GA generation must still be made. In this work, a linear problem was solved to generate this initial guess of nodal deflections. However, it was found that when the forces were an order of magnitude apart, this guess still gave a large number (greater than 5%) of nonconvergent nonlinear FEA iterations. With a lower allowable actuation force, on the other hand, the relative motion and shape of the deformed wing are close to those desired, but the achieved absolute deflections are lower. Thus, to ease convergence of nonlinear FEA as well as to achieve high deflections, a low actuation-force range was first used in the GA to achieve an optimal topology. A multiplication factor was then used on the cable actuation forces of the optimal topology. Such a scheme resulted in uniform displacement as well as ease of convergence. Two cases are presented for the HECS wing. The first uses a low actuation-force range, and the second uses a larger range. The results are presented in the following subsections.

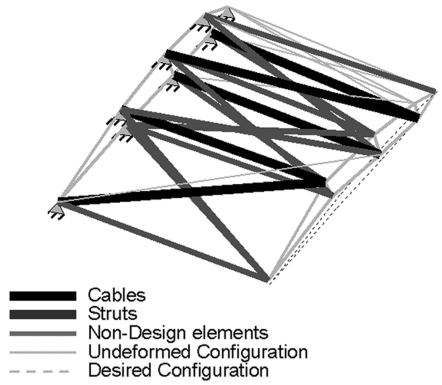

Fig. 7 Resultant deflection: actuation-force multiplication factor of 75.

Table 2 Fitness values: results 1, 2 and 3

Result no.	f_1	f_2
1	0.0140	0.00078
2	0.0141	0.00067
3	0.0142	0.00039

Table 3 Leading-edge nodal deflections: result 1

Leading edge	Span change (as % of original span)	Thickness change (as % of original thickness)	Chord change (as % of original chord)
Obtained	0.0005	1.524	0.033
Desired	0.005	120.95	0

Table 4 Fitness values: 75 × F_{act}

Actuation force	f_1	f_2
F_{act}	0.0140	0.00078
1 75 × F_{act}	0.00757	0.00078

Table 5 Fitness values

Actuation force	f_1	f_2
F_{act}	0.0125	0.00081
4.8 × F_{act}	0.00746	0.00081

A. Case I: Low Actuation-Force Range

In case I, the actuation force in each of the cables is allowed to vary between 0.2 and 200 lb. Hence, each cable in the optimal topology can be actuated by different amounts. The cable actuation ranges are chosen such that they are close in magnitude to the aerodynamic loads, thereby facilitating convergence of the nonlinear finite element analysis. With a starting guess for the nodal deflections as discussed in Sec. IV, a very small fraction of the nonlinear FEA runs (0.025% out of 300,000 nonlinear FEA runs) were found to be nonconvergent. This problem was solved on an 81-node (162 AMD Athlon MP 2200 CPUs) cluster with a main memory of 2 GB for 18 nodes, and 1 GB for the other nodes. Each GA generation in case I takes an average of 4.6 s to run. Hence, a run of 500 generations with a population size of 300 takes about 40 min. The initial ground structure for the HECS wing along with the output points is shown in Fig. 5. The desired morphed configuration is shown with the dotted line.

The Pareto front showing the tradeoff between the two objectives is given in Fig. 6a along with three sample Pareto points (shown by three points) on the curve. These three points are picked to study the difference between the final topologies for different fitness values. The three optimal topologies for the three sample points are shown in Figs. 6b–6d. The dashed line shows the desired morphed configuration. Table 2 gives the fitness values for the three results.

Result 1 (Fig. 6b) has the best fitness in terms of deflection under actuation and airloads, and result 3 (Fig. 6d) has the best fitness (stiffness) under airloads, although the topologies and the fitness values are not very different from each other. This indicates that the final solution set shows a set of results that are very close to each other and not too diverse in nature. Result 1 was selected as the best result for further analysis, because it has the maximum deflection under actuation.

Result 1 consists of 5 cables, 12 struts, and 7 voids. The strains in the cables are -4.4×10^{-6}, -1.3×10^{-5}, -4.4×10^{-6}, 0, and 0. The cable actuation forces are 0.7, 76.1, 195.7, 184.5, and 196 lb. Table 3 compares the desired and achieved nodal deflections of the node on the leading edge. The achieved deflection is clearly lower than desired. To achieve larger deflection, the cable actuation forces were multiplied by various scaling factors ranging from 2 to 100. The best results were achieved when using a scaling factor of 75. The stress constraints were still satisfied with the actuation-force multiplication factor of 75. The resultant deflection with a scaling factor of 75 is shown in Fig. 7. The leading- and trailing-edge deflections are close to their desired values. However, some local deformation of the airfoil is observed.

Table 6 Leading-edge nodal deflections: case II

Leading edge	Span change (as % of original span)	Thickness change (as % of original thickness)	Chord change (as % of original chord)
Obtained	0.0005	6.286	0.088
Desired	0.005	120.95	0

The increase in actuation force decreases the error between the desired and achieved deformations (f_1). Thus, the solution gets closer to the desired solution. Hence, by scaling up the actuation force, the deflection is increased, and the increase occurs in the expected direction. Table 4 gives the objective function under actuation and airloads (f_1) and under airloads only (f_2). It is found that the error under actuation and airloads is much smaller in the 75 × actuation force case when compared with the error value in the unscaled case.

B. Case II: High Actuation-Force Range

In case II, the upper limit of the cable actuation force is increased by a factor of 10, which was chosen because the resultant number of nonconvergent iterations from the nonlinear finite element analysis was low (less than 5% of the total number of function evaluations). Any further increase in the cable actuation force causes a significant increase in the fraction of nonconvergent nonlinear FEA. Hence, in

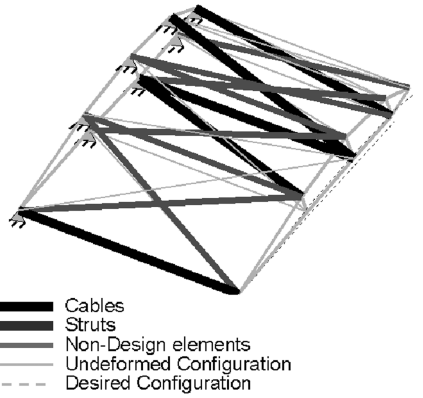

Fig. 9 Wing deformation: actuation-force scaling factor of 4.8.

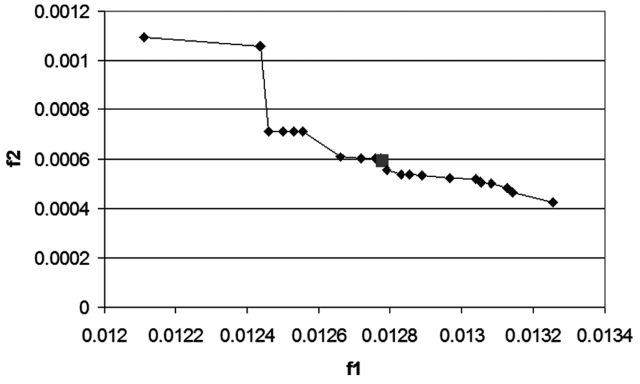

a) Pareto front

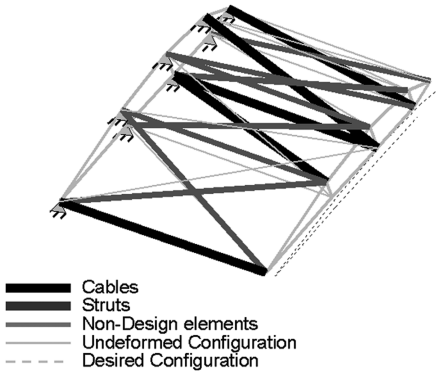

b) Optimal topology

Fig. 8 Optimization results: case II.

this case, an actuation-force range of 0.196 to 1960 lb is allowed. The average time taken per GA generation is larger than in case I and is equal to 10.7 s. Hence, for 500 generations, the problem runs for 1.5 h. The number of nonconvergent iterations from the nonlinear FEA in case II is higher than case I (2.7% as compared with 0.025% of case I). As explained earlier, this is due to the large actuation-force range. The resultant Pareto front and sample Pareto point optimal topology are shown in Fig. 8. The final topology consists of 8 struts, 5 cables and 11 void elements. The cable actuation forces are 1811.7, 110.1, 1889.6, 1929.4, and 1896.5 lb. The fitness values are given in the first row of Table 5.

Thus, the error under actuation with airloads is lower than the error in case I. A comparison between the desired and achieved leading-edge nodal deflections is given in Table 6. The deflections are lower than desired. However, by using a scaled-up value of the cable actuation forces, higher deflection is achieved. To study this, cable actuation forces are scaled up by factors ranging from 2 to 5. The maximum scaling factor is chosen as 5, because convergence of nonlinear FEA is not achieved for higher scaling factors. The best results are achieved when the cable actuation force is multiplied by a factor of 4.8. The error in f_1 value decreases, as shown in the second row of Table 5. The stress constraints are satisfied with the additional actuation force. The deformation of the wing with a scaling factor of 4.8 (Fig. 9) is quite uniform.

From the results, good error reduction is achieved when using higher actuation forces. However, most of the improvement is obtained indirectly using a scaled actuation force rather than a direct higher limit on actuation force in the optimization. It is also easiest to achieve convergence of the nonlinear FEA iteration when using a low actuation-force range. Stress constraints are satisfied in the original, as well as the scaled, actuation-force topologies.

VI. Conclusions

This paper presents a methodology for the optimal design of morphing aircraft wings. The problem formulation considers a multi-objective, multiconstraint, and discrete continuous set of design variables. A very computationally intensive problem is considered and solved using NSGA II (parallelized as part of this work). Nonlinear FEA was used to address the large deformation requirements of the problem.

Although parallelization reduces computation time and, in the present case, is absolutely essential to obtain a solution at all, it causes other time issues, such as queue wait time, queue time limit, and processor communication time. Hence, the effort is justified only if the time to run the serial program is unacceptable.

Convergence of nonlinear FEA was also found to be an issue. Schemes have been suggested in the current work to speed up convergence. However, the same scheme does not work for every problem; suitable schemes are problem-specific. Hence, different schemes have to be evaluated to find one that facilitates quick convergence of the nonlinear FEA for the problem at hand.

Good agreement between the desired and achieved configurations were obtained for the HECS wing when the cable actuation force was scaled up. From the results, good error reduction is achieved using high actuation forces. However, in case II, in which a higher actuation-force range was allowed as part of the design, convergence issues related to the nonlinear FEA were encountered. This comes from the fact that with a high allowable actuation force, the actuation forces become an order of magnitude higher than the aerodynamic loads, making the convergence of nonlinear FEA difficult. A better approach for improving the convergence of nonlinear FEA is to use a ramped-up actuation force, as in case I, rather than allowing a large actuation-force range to the optimizer.

From the optimization results, the required actuation forces were found to be quite large. This may be undesirable, because considerable actuation effort would be needed to produce the desired motion. One way to address this issue is to consider the actuation force in the objective. Future work may involve minimizing the cable actuation force. Weight is an important consideration in the design of a morphing aircraft wing. Future work may be directed toward using weight as an objective function, with the element cross-sectional areas as possible design variables. Additionally different ground structures may be used to potentially achieve better results. A GA parametric study may also be used to increase diversity of the GA population.

Appendix A: Flow Diagram and Equations for Nonlinear FEA

An iterative full Newton–Raphson procedure is used for determining the state of force equilibrium. The flow diagram is shown in Fig. A1.

As explained in Sec. IV, nonlinear FEA involves finding values of nodal deflections such that Eq. (A1) is satisfied:

$$F - R = 0 \tag{A1}$$

At the start of the N-R procedure, an initial guess for U is made. The following equations are used for calculation of the residual $(F - R)$. The first step involves calculation of strain. Green's strain is used as a strain measure. It is given by Eq. (A2):

$$\varepsilon_G = \frac{l_n^2 - l_0^2}{2l_0^2} \tag{A2}$$

For a truss element, the longitudinal Green's strain is given by Eq. (A3):

$$\varepsilon_G = b_1^T p + 0.5 b_2^T p \tag{A3}$$

For a three-dimensional element, the strain-displacement relationships b_1 and b_2 are given by Eqs. (A4) and (A5):

$$b_1^T(x) = \frac{1}{\alpha_0^2}(Ax_1)^T \tag{A4}$$

$$b_2^T(p) = \frac{1}{\alpha_0^2}(Ap)^T \tag{A5}$$

A is a matrix given by Eq. (A6):

$$A = \frac{1}{4}\begin{bmatrix} 1 & -1 & 0 & 0 & 0 & 0 \\ -1 & 1 & 0 & 0 & 0 & 0 \\ 0 & 0 & 1 & -1 & 0 & 0 \\ 0 & 0 & -1 & 1 & 0 & 0 \\ 0 & 0 & 0 & 0 & 1 & -1 \\ 0 & 0 & 0 & 0 & -1 & 1 \end{bmatrix} \tag{A6}$$

The second term in Eq. (A3) gives the nonlinear part of the strain. Once Green's strain is calculated, the stress is calculated simply by Eq. (A7):

$$\sigma = E\varepsilon_G \tag{A7}$$

The principle of virtual work is used to find the internal forces q_i. The expression for q_i is given by Eq. (A8) [12]:

$$q_i = 2\alpha_0 A_0 \sigma b \tag{A8}$$

Here, $b = b_1 + b_2$ from Eqs. (A4) and (A5). Equation (A8) gives the internal nodal forces for a strut element. For an actuating element,

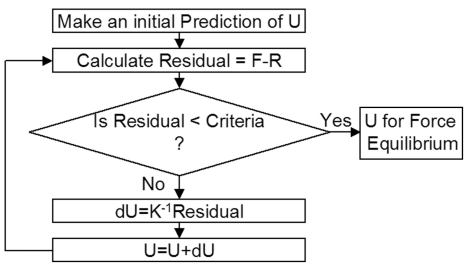

Fig. A1 The N-R procedure flow diagram.

Eq. (A8) is used as before. However, instead of σ, σ_{act} is used. The σ_{act} (stress due to actuation) is given in Eq. (A9):

$$\sigma_{\text{act}} = E\varepsilon_{\text{act}} = CV \tag{A9}$$

In calculating the strain due to actuation, the strain in the cable is assumed to be proportional to the applied actuation V, and C is the constant of proportionality. In Eq. (A1), F is q_i due to σ, and R is the sum of aerodynamic loads and q_i due to σ_{act}. Once the residual has been calculated, the next step (Fig. A1) is to determine dU in case the residual is greater than the convergence criteria. This is calculated using Eq. (A10):

$$dU = K^{-1} \times \text{residual} \tag{A10}$$

The tangent stiffness matrix K corresponds to the geometric and material conditions of the structure. It is given by Eq. (A11):

$$K_t = K_{t1} + K_{t2} + K_{t\sigma} \tag{A11}$$

The expressions for the preceding stiffness terms are given in Eqs. (A12) and (A13):

$$K_{t12} = K_{t1} + K_{t2} = 2E\alpha_0 A_0 bb^T \tag{A12}$$

$$K_{t\sigma} = \frac{2A_0\sigma}{\alpha_0} A \tag{A13}$$

In the next step of the flow diagram shown in Fig. A1, U is updated by Eq. (A14):

$$U = U + dU \tag{A14}$$

This process is iteratively repeated until convergence is achieved.

Acknowledgments

The authors gratefully acknowledge the support of the U.S. Air Force Office of Scientific Research, Structural Mechanics Program, under grant FA9550-05-1-0165. The authors also thank NASA for supplying the aerodynamic load data and the morphing specifications for the hyper-elliptic camber section (HECS) wing.

References

[1] Kudva, J. N., Sanders, B., Pinkerton-Florance, J., and Garcia, E., "The DARPA/AFRL/NASA Smart Wing Program—Final Overview," *Smart Structures and Materials 2002—Industrial and Commercial Applications of Smart Structures Technologies*, Proceedings of SPIE, Vol. 4698, Society of Photo-Optical Instrumentation Engineers, Bellingham, WA, Mar. 2002, pp. 37–43.

[2] Kudva, J. N., Sanders, B., Pinkerton-Florance, J., and Garcia, E., "Overview of the DARPA/AFRL/NASA Smart Wing Phase 2 Program," *Smart Structures and Materials 2001—Industrial and Commercial Applications of Smart Structures Technologies*, Proceedings of SPIE, Vol. 4332, Society of Photo-Optical Instrumentation Engineers, Bellingham, WA, Mar. 2001, pp. 383–389.

[3] Ramrakhyani, D. S., Lesieutre, G., Frecker, M. I., and Bharti, S., "Aircraft Structural Morphing Using Tendon-Actuated Compliant Cellular Trusses ," *Journal of Aircraft*, Vol. 42, No. 6, Nov.–Dec. 2005, pp. 1614–1620. doi:10.2514/1.9984

[4] McGowan, A.-M. R., Washburn, A. E., Horta, L. G., Bryant, R. G., Cox, D. E., Siochi, E. J., Padula, S. L., and Holloway, N. M., "Recent Results from NASA's Morphing Project," *Smart Structures and Materials 2002—Annual International Symposium on Smart Structures and Materials*, Proceedings of SPIE, Vol. 4698, Society of Photo-Optical Instrumentation Engineers, Bellingham, WA, Mar. 17–21 2002, pp. 97–111.

[5] Bharti, S., Frecker, M. I., Lesieutre, G., and Browne, J., "Tendon Actuated Cellular Mechanisms for Morphing Aircraft Wing," *Modeling, Signal Processing and Control for Smart Structures 2007*, Proceedings of SPIE, Vol. 6523, Society of Photo-Optical Instrumentation Engineers, Bellingham, WA, 15–18 Mar. 2007, Paper 652307.

[6] Wiggins, L. D., Stubbs, M. D., Johnston, C. O., Robertshaw, H. H., Reinholtz, C. F., and Inman, D. J., "A Design and Analysis of a Morphing Hyper-Elliptic Cambered Span (HECS) Wing," *AIAA/ASME/ASCE/AHS/ASC Structures, Structural Dynamics and Materials Conference*, Vol. 5, AIAA, Reston, VA, 2004, pp. 3979–3988.

[7] Raymer, D. P., "Structures and Loads," *Aircraft Design: A Conceptual Approach*, 4th ed., AIAA, Reston, VA, 2006, pp. 404–410.

[8] Deb, K., Pratap, A., Agarwal, S., and Meyarivan, T., "A Fast and Elitist Multiobjective Genetic Algorithm: NSGA II," *IEEE Transactions on Evolutionary Computation*, Vol. 6, No. 2, Apr. 2002, pp. 182–197. doi:10.1109/4235.996017

[9] Deb, K., "Elitist Multi-Objective Evolutionary Algorithms," *Multi-Objective Optimization Using Evolutionary Algorithms*, 1st ed., Wiley-Interscience Series in Systems and Optimization, Wiley, New York, 2001, pp. 245–253.

[10] Pacheco, P. S., "Advanced Point-to-Point Communication," *Parallel Programming with MPI*, Morgan Kaufmann, San Francisco, 1997, pp. 279–314.

[11] Bathe, K. J., "Finite Element Nonlinear Analysis in Solid and Structural Mechanics," *Finite Element Procedures*, Prentice–Hall, Englewood Cliffs, NJ, 1996, pp. 485–566.

[12] Crisfield, M. A., "Truss Elements and Solutions for Different Strain Measures," *Non-Linear Finite Element Analysis of Solids and Structures*, Wiley, New York, 1991, pp. 57–72.

[13] Esche, S. K., Kinzel, G. L., and Altan, T., "Issues in Convergence Improvement for Nonlinear Finite Element Programs," *International Journal for Numerical Methods in Engineering*, Vol. 40, No. 24, Dec. 1997, pp. 4577–4594. doi:10.1002/(SICI)1097-0207(19971230)40:24<4577::AID-NME273>3.0.CO;2-D

[14] Bendsoe, M. P., and Sigmund, O., "Extensions and Applications," *Topology Optimization: Theory, Method and Applications*, Springer, Berlin, 2003, pp. 86–90.

[15] Chung, K., and Wagoner, R. H., "Numerical Improvement of Viscoplastic, Nonlinear, Finite Element Analysis," *International Journal of Mechanical Sciences*, Vol. 29, No. 1, 1987, pp. 45–59. doi:10.1016/0020-7403(87)90073-7

E. Livne
Associate Editor